Binary Phases of Aliphatic *N*-Oxides and Water: Force Field Development and Molecular Dynamics Simulation

Kristine M. Kast,[†,‡] Jürgen Brickmann,[†] Stefan M. Kast,*[,†,§] and R. Stephen Berry[§]

Physikalische Chemie I, Technische Universität Darmstadt, Petersenstrasse 20, 64287 Darmstadt, Germany, and Department of Chemistry, The University of Chicago, 5735 South Ellis Avenue, Chicago, Illinois 60637

Received: October 29, 2002; In Final Form: April 23, 2003

Aliphatic *N*-oxides as cosolvents with water play an important role in stabilizing and destabilizing the structure of biopolymers such as cellulose and proteins. To allow for detailed microscopic investigations, an empirical force field to be used in molecular simulations is developed for two *N*-oxide species, *N*,*N*,*N*-trimethylamine-*N*-oxide (TMAO) and *N*-methylmorpholine-*N*-oxide (NMMO). The intra- and intermolecular force field is parametrized mainly on the basis of quantum-chemical calculations and is tested against available experimental spectroscopic, crystallographic, and liquid state data. Special emphasis is put on the identification of transferable potential terms in order to guide future parametrization of other species. By construction, the force field is compatible with widely used potential functions for proteins and carbohydrates. With the resulting parameter set, molecular dynamics simulations are carried out on binary mixtures of water and *N*-oxides, revealing structural features and the influence of intramolecular *N*-oxide flexibility. Limitations and possible extensions of the presented models are also discussed.

I. Introduction

The unique properties of solvent mixtures as compared to pure phases play an increasingly important role for industrial applications, e.g., for tuning solubility or reactivity by introducing the mole fraction as an additional control variable. Furthermore, the biochemical relevance of dissolved compounds in water is an important aspect of current research on protein stability and biomolecular recognition. Tertiary aliphatic *N*-oxides are remarkable species in these respects: Some are known as good cosolvents with water for dissolving cellulose fibers,[1−6] increasing the reactivity of the swollen cellulose material for further derivatization in pollution-free industrial fiber processing. For instance, *N*-methylmorpholine-*N*-oxide (NMMO) in water dissolves cellulose, whereas *N*,*N*,*N*-trimethylamine-*N*-oxide (TMAO) does not.[7] On the other hand, TMAO abounds in marine organisms as an osmolyte counteracting protein denaturation provoked by urea and related osmotic water stress[8,9] or by high-pressure conditions.[10] TMAO even appears to play a role in possible therapies for Alzheimer's disease.[11] Explanations on the molecular level for these phenomena are only beginning to surface.[12−19]

To investigate into the molecular mechanism of these effects by computational methods such as molecular dynamics (MD) simulation techniques, a force field for mixed solvents composed of water and *N*-oxide species is required that is also compatible with available biopolymer potential energy functions. Noto et al.[20] were the first who constructed a force field for a rigid TMAO model in the presence of an aqueous environment based on quantum-chemical calculations of TMAO and a single water molecule within the Hartree−Fock (HF) approximation. The TMAO-water interaction potential comprises a modified Coulomb term and a $r^{-10}/r^{-4}/r^{-2}$ expression covering dispersion and repulsion where r means the site−site distance and has not been tested with respect to its performance for reproducing condensed phase experimental data. The force field was then used in MD simulations of a single TMAO molecule in water.[20] Zou et al. applied the force field with some adjustments in simulations at finite TMAO concentrations.[19] They found some evidence regarding changes of water−water structure and dynamics due to the *N*-oxide presence and related this result to the protein stabilization effect. Besides this early TMAO force field, quite recently a model potential function for studying intramolecular H-bond dynamics in picolinic acid *N*-oxide has been constructed and applied to the computational treatment of spectroscopic experiments.[21,22]

In this work, a force field for two prototypical *N*-oxides, TMAO and NMMO, is developed and tested for its capability to reproduce experimental data. It is intended to be balanced in the sense of satisfying several requirements: (1) The functional form and the parameters should be compatible with common water models and biopolymer force fields such as CHARMM[23−25] for proteins and extensions for carbohydrates;[26] (2) the force field should be as simple as possible to avoid overly expensive computations for simulating the solvent, yet account for intramolecular flexibility; (3) certain terms in the force field that represent topologically similar units should be attributed identical, i.e., transferable parameters guiding future parametrization of other *N*-oxide species; (4) it should be applicable for a range of different situations such as various concentrations. Because experimental information about *N*-oxide systems is very limited, the parametrization relies mainly on quantum-chemical calculations. The adequate approximations, like basis set and inclusion of electron correlation, have been outlined in the past by some of us for a number of different *N*-oxide/water systems.[27] Although several parameters can be directly deduced from these resources, the parametrization of a solvent force field containing

* To whom correspondence should be addressed. E-mail: kast@pc.chemie.tu-darmstadt.de. Phone: +49 6151 165397. Fax: +49 6151 164298.

† Technische Universität Darmstadt.

‡ Present address: T-Systems GEI GmbH, Goebelstr. 1-3, 64293 Darmstadt, Germany.

§ The University of Chicago.

10.1021/jp027336a CCC: $25.00
Published on Web 06/14/2003

flexible molecular entities constitutes a major challenge. In the next sections, we first describe the model function and the strategy toward useful parameters along with the results. The model is validated by comparison with crystallographic and spectroscopic as well as liquid state data from experiments and is finally applied to equimolar *N*-oxide/water mixtures, revealing liquid-phase structural features and the influence of intramolecular flexibility.

II. Force Field Parametrization

(a) Outline. Force field development, particularly for complex condensed phase systems, is a challenging task, often guided more by experience in conducting the appropriate steps than by straightforward recipes; for recent reviews, see refs 28−30 The model potential used in this work has the form

$$U = \sum_{\text{bonds}} \frac{k_r^{ab}}{2}(r_{ij} - r_0^{ab})^2 + \sum_{\text{angles}} \frac{k_\alpha^{abc}}{2}(\alpha_{ijk} - \alpha_0^{abc})^2 - \frac{k_r^{ac}}{2}(r_{ik} - r_0^{ac})^2 + \sum_{\text{torsions}} \sum_n k_{\tau,n}^{abcd}[1 + \cos(n\tau_{ijkl} - \tau_0^{abcd})] + \sum_{j>i} U_{\text{nb}}^{ab}(r_{ij}, r_c) \quad (1)$$

where the first three terms define an intramolecular valence force field and the last term the nonbonded contributions, including intermolecular interactions. Superscripts $a-d$ denote atomic types by requirements of topological equivalence, and subscripts $i-l$ refer to particular atomic site indices. The intramolecular valence force field consists of harmonic terms for bond stretching (site distance r_{ij}, force constant k_r, and equilibrium distance r_0) and angle bending (bend angle α, force constant k_α, and equilibrium angle α_0), and a torsional potential defined over cosines of the dihedral angle τ (multiplicity n, phase τ_0, and torsional parameter $k_{\tau,n}$ that is just half the energy barrier). For fine-tuning the normal frequencies, additional Urey−Bradley terms are introduced comprising a harmonic potential along the distance between the first and the third atom of a bend angle. The nonbonded potential is described basically by the sum of Coulomb interaction (nonpolarizable partial site charges q, dielectric constant ϵ_0) and a Lennard-Jones term (well depth ϵ, contact distance σ; standard Lorentz−Berthelot combinations rules[31] are used: $\epsilon^{ab} = (\epsilon^a \epsilon^b)^{1/2}$, $\sigma^{ab} = (\sigma^a + \sigma^b)/2$)

$$U_{\text{nb}}^{ab}(r_{ij}) = \frac{q^a q^b}{4\pi\epsilon_0 r_{ij}} + 4\epsilon^{ab}\left[\left(\frac{\sigma^{ab}}{r_{ij}}\right)^{12} - \left(\frac{\sigma^{ab}}{r_{ij}}\right)^{6}\right] \quad (2)$$

for all atoms pairs in different molecules as well as in the same molecule if they are separated by three or more bonds. Throughout, nonbonded interactions except for intramolecular distances are modified by multiplication with[23,32] $(1 - (r_{ij}/r_c)^2)^2$ using a truncation distance r_c discussed later. For reasons of computational performance, this form has been used for both the Lennard-Jones and the Coulomb term; the energetic difference as compared to applying more elaborate and computationally more demanding Lennard-Jones shifting techniques[32] is negligibly small for such strongly polar systems.

An appropriate strategy for finding suitable parameters for the model compounds TMAO and NMMO (the structure and site numbering is shown in Figure 1) consists of several consecutive stages: First, the site charges were determined from quantum-chemical ab initio calculations of isolated *N*-oxides; the remaining nonbonded parameters were adjusted to represent structure and energetics of *N*-oxide hydrates from ab initio and experimental crystal data. Second, the torsional potentials were fitted to quantum-chemical barriers, and finally, the remaining valence force field terms were determined by adjusting to structural and vibrational results again from ab initio calculations. The final potential was then tested against experimental condensed phase properties by MD simulations. The force field is largely inspired by the CHARMM approach,[23−25] in particular we use, at least as initial estimates, known parameters from the CHARMM force field whenever possible. By construction of the consecutive parametrization steps, the nonbonded parameters influence the intramolecular ones and not vice versa, so some compatibility to other force fields based on pairwise site−site intermolecular interactions can be expected. Parameters that turn out to be very similar upon individual optimization of similar molecular groups will be set equal if possible without significant loss of accuracy, thereby allowing for the identification of basic building blocks to be used in other *N*-oxides. The key developments involve the region around the N−O bond that is difficult to handle as we will see.

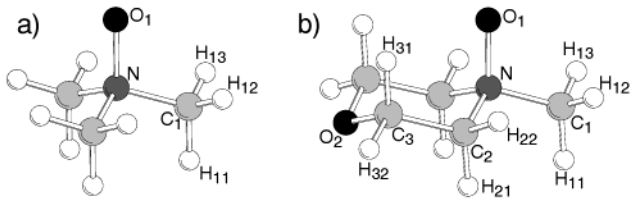

Figure 1. Structure and site indices for TMAO (a) and NMMO (b).

Quantum chemical ab initio calculations were performed with the Gaussian suite of programs.[33] The appropriate level of theory has been analyzed in depth in an earlier study:[27] Although the HF approximation with the 6-31G** basis set is suitable for pure compounds, water complex properties need computations on the MP2 level (Møller−Plesset perturbation theory to second order) for correctly representing experimental H-bond energies. *N*-oxide/water complex interactions energies were corrected by the basis set superposition error (BSSE) according to Boys and Bernadi.[34] MD simulations were conducted in the isothermal−isobaric (*NpT*) ensemble[35,36] at a pressure of 1 bar and various temperatures, using a time step of 1 fs and periodic boundary conditions throughout and applying distance constraints when necessary.[37,38] The numerical parametrization work was done for a large part with a dynamical simulated annealing optimization method described earlier.[28,39]

(b) Partial Charges. Based on results of earlier ab initio investigations,[27] atomic site charges were determined by fitting to the electrostatic potential (ESP charges) rather than from population analysis. The latter (see also ref 20) yields quite unphysical values particularly for the central N atom that carries a positive formal charge. We used gas phase results instead of, for instance, quantum-chemical reaction field techniques to allow for electronic polarization due to the environment in order to maintain compatibility with the parametrization strategy commonly used for solute species. Furthermore, for such a nonpolarizable force field as used in this work, we would need representative environment models for a broad range of molar ratios between solvent and cosolvent. To allow for rotatable methyl groups the hydrogen charges were averaged, also for the NMMO methylene groups. Table 1 shows the dipole moments for both the HF and the MP2 level of theory together with result from the respective point charge distribution, and experimental values[40,41] for TMAO. As can be seen, dipole moments taken directly from the wave function are quite similar for HF and MP2, and the HF result is closer to the experimental

TABLE 1: Dipole Moments μ Resulting from Wave Function and Point Charge Distributions on Various Levels of Theory

	μ(TMAO)/Debye	μ(NMMO)/Debye
wave function (MP2)	4.660	3.663
wave function (HF)	4.916	3.858
point charges (MP2)	5.287	3.505
point charges (HF)	5.733	3.621
exp (in benzene)	5.02,[40] 4.87[41]	

TABLE 2: Assignment of Atom Types and Partial Charges to the *N*-Oxides[a]

compound	atom	atom type	charge/*e*
TMAO	O_1	ON1	−0.65
	N	NN1	0.44
	C_{1a}, C_{1b}, C_{1c}	CT3N1	−0.26
	H_{11a-c}, H_{12a-c}, H_{13a-c},	HAN1	0.11
NMMO	O_1	ON2	−0.67
	N	NN2	0.44
	C_1	CT3N2	−0.33
	C_{2a}, C_{2b}	CT2N	−0.11
	C_{3a}, C_{3b}	CT2NM	0.24
	O_2	ONM	−0.50
	H_{11}, H_{12}, H_{13}	HAN2	0.13
	$H_{21a,b}$, $H_{22a,b}$	HAN2	0.06
	$H_{31a,b}$, $H_{32a,b}$	HA	0.06

[a] Subscripts a−c denote atoms in topologically equivalent methyl/methylene groups.

values for TMAO. However, the HF point charge result deviates strongly in the TMAO case. Therefore, the HF-derived point charges were used for NMMO only and the MP2 ones for TMAO. The final charges are given in Table 2 along with the assigned atom type symbols used later.

With the resulting partial charges, the potential truncation distance was optimized using a procedure developed by Dufner et al.:[42] Forces and energies from direct summation of the shifted-force potential were compared with Madelung values from Ewald summation[43] in the case of the experimental TMAO crystal structure.[44] For a cutoff distance, r_c, of 13 Å, directly summed energies deviate by less than 2% and forces less than 1% from the true Madelung values. This truncation distance has then been used throughout. From earlier experiences with cutoff distances optimized in this way,[39] we can expect structural deviations with respect to results from crystal simulations applying the Ewald summation technique of around 1−2%.

(c) Lennard-Jones Parameters. Because no explicit polarizability was taken into account, the remaining nonbonded parameters were designed to reflect the effective many-body interactions mapped on simple site−site interactions. The Lennard-Jones parameters in the N−O region were adjusted to geometrical and energetic reference data from ab initio calculations on *N*-oxide hydrates. The dominant structural motif found in the experimental crystal structures can be reproduced by geometry optimization of TMAO and NMMO dihydrates on the MP2 level (see Figure 2). In this case, the internal *N*-oxide geometries were frozen on the previous results,[27] and the water structure and potential was represented by the rigid three-site TIP3P model[45,46] with small Lennard-Jones parameters attributed to the hydrogens.[47] The parameters of the atoms in the N−O region including attached methyl and methylene groups were then adjusted by simulated annealing[28,39] in order to reproduce the optimal dihydrate geometries. Each atom sort was assigned the same parameters, taken to be transferable between TMAO and NMMO.

As a result, illustrated in Figure 2, rms deviations between matched[48] dihydrate structures from ab initio and force field

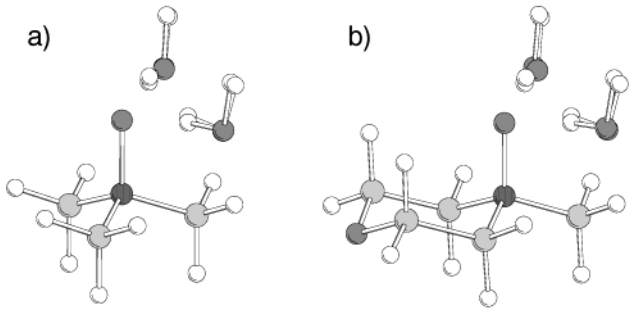

Figure 2. Superposition of optimized ab initio and force field structures of dihydrates of TMAO (a) and NMMO (b).

TABLE 3: Lennard-Jones Parameters of the Atom Types

type	ϵ/kcal mol^{-1}	σ/Å
ON1, ON2	0.1526	3.266
ONM	0.0884	2.891
NN1, NN2	0.2000	2.926
CT3N1, CT3N2, CT2N	0.0676	3.041
CT2NM	0.0655	3.978
HAN1, HAN2	0.0185	1.775
HA	0.0220	2.352

calculations are 0.045 Å for TMAO and 0.056 Å for NMMO with the final Lennard-Jones parameters summarized in Table 3. The BSSE-corrected quantum-chemical and resulting force field interaction energies (computed on the ab initio structures) are for TMAO dihydrate −20.04 and −19.57 kcal mol^{-1}, respectively, and for NMMO dihydrate −18.70 and −19.31 kcal mol^{-1}. A number of other mono- and dihydrate structures have been computed yielding a rms deviation between BSSE-corrected MP2 energies and force field values of around 0.9 kcal mol^{-1}, so no further parameter adjustment was deemed necessary.

It turned out that the force field dihydrate structures tend to break C_s symmetry by bending the water planes synchronously toward the methyl/methylene groups plane upon geometry optimization, regardless of the parameters. Because this effect was not observed for the ab initio structures, we can attribute it to a lack of flexibility, i.e., the nonpolarizability, of the model potential, expected to be large at the *N*-oxide oxygen. Improvement could possibly be achieved by using off-site charge centers on the oxygen atom, reflecting to some extent charge transfer into the water hydrogen directions. Both possible remedies, adding explicit polarizability[49,50] or off-site charge centers for flexible entities, would mean a significant complication of the model and higher computational demand. We therefore refrained from such extensions and used constraints for keeping the water molecules upright during geometry optimizations, mimicking the directional forces induced by the H-bonding environment in a condensed phase.

The ether group in the morpholine ring ($-CH_2-O-CH_2-$), the Lennard-Jones parameters of which were set to standard values of the CHARMM parameter set up to this point, needed some further refinement: The associated parameters were slightly modified by a Newton−Raphson[51] minimization of a penalty function

$$S(\boldsymbol{\varphi}) = \sum_i (\langle O_i \rangle - O_{i,\mathrm{ref}})^2 \qquad (3)$$

that measures the deviation of thermally averaged observables $O_i(\boldsymbol{\varphi})$ depending on a number of parameters $\boldsymbol{\varphi}$ from reference values $O_{i,\mathrm{ref}}$. In our case, the crystallographic cell parameters of NMMO monohydrate act as observables, with reference

TABLE 4: Torsional Parameters k_τ^{abcd} [a]

type (*a*)	type (*b*)	type (*c*)	type (*d*)	k_τ^{abcd}/kcal mol^{-1}
ON1	NN1	CT3N1	HAN1	0.27
ON2	NN2	CT3N2	HAN2	0.27
ON2	NN2	CT2N	HAN2	0.27
ON2	NN2	CT2N	CT2NM	0.27
CT3N1	NN1	CT3N1	HAN1	0.27
CT3N2	NN2	CT2N	HAN2	0.27
CT3N2	NN2	CT2N	CT2NM	0.27
NN2	CT2N	CT2NM	ONM	0.20
NN2	CT2N	CT2NM	HA	0.20
CT2N	NN2	CT3N2	HAN2	0.27
CT2N	NN2	CT2N	HAN2	0.27
CT2N	NN2	CT2N	CT2NM	0.27
CT2N	CT2NM	ONM	CT2NM	0.15
HAN2	CT2N	CT2NM	ONM	0.15
HAN2	CT2N	CT2NM	HA	0.15
HA	CT2NM	ONM	CT2NM	0.10

[a] Multiplicity $n \equiv 3$, phase $\tau_0 \equiv 0$; $a-d$ denote adjacent atoms constituting a dihedral angle.

values taken from the literature[52] and thermal averages obtained from MD simulations with the rigid molecules used up to this point. Also, the necessary first and second derivatives of *S* with respect to nonbonded parameters were approximated by finite differences, deduced from a number of 48 ps simulations at 298.15 K and 1 bar with small variations of the Lennard-Jones parameters applied to a crystal section comprising 384 water and NMMO molecules. It turned out that the cell parameters are only weakly sensitive to a variation of the ether group nonbonded parameters, so the optimization was terminated after a single Newton−Raphson step. The resulting parameters are also found in Table 3.

(d) Torsional Parameters. Starting from HF-optimized *N*-oxide geometries with imposed local C_3 symmetry of the methyl groups, the ab initio torsional energy profile was computed on the MP2 level by varying the O−N−C−H dihedral angle in steps of 30°, keeping all other coordinates fixed. The corresponding force field barriers, to be expressed by the torsional potential terms, were then computed from the difference of ab initio energies and the model potential known so far. To this end, inclusion of 1−4 Coulomb plus Lennard-Jones as well as only 1−4 Lennard-Jones interactions, both without further scaling, were compared. The energy barriers obtained are very similar for TMAO and NMMO in both cases, including only 1−4 Lennard-Jones terms (TMAO 0.540 kcal mol^{-1}, NMMO 0.537 kcal mol^{-1}) or including both Lennard-Jones and Coulomb interactions (TMAO 0.506 kcal mol^{-1}, NMMO 0.506 kcal mol^{-1}). To allow for transferability to other *N*-oxides with different charge distributions, torsional parameters obtained from the calculations including only 1−4 Lennard-Jones contributions were derived for the further parametrization process.

Assuming equal contributions to the total barrier, the individual terms were distributed (for instance one H−C−N−C and two H−C−N−O terms for each of three hydrogen atoms in one methyl group, the result multiplied by three gives the total barrier) and averaged for TMAO and NMMO. Force field contributions to the dihedral potential within the NMMO morpholine ring were described by standard CHARMM and carbohydrate[26] parameters for similar torsions. In this way, the methyl group rotation is correctly described in all cases, whereas the torsion contribution to the intraring flexibility of NMMO influences the normal vibrations that are optimized in the next section by adjusting the remaining parameters. All torsional parameters are listed in Table 4.

The set of intermolecular and torsional potential terms allowing only for methyl group rotation constitutes a partly rigid model to be examined and contrasted with the fully flexible model in more detail later. We do not consider the inherently quantal nature of methyl group rotations in our model. The rigid substructure coordinates are given in Tables 5 and 6; the remaining constraint distances are $d(\mathrm{N-H_{11,12,13}}) = 2.090$ Å (TMAO)/2.087 Å (NMMO), $d(\mathrm{C_1-H_{11,12,13}}) = 1.081$ Å (TMAO/NMMO), and $d(\mathrm{H_{11}-H_{12}}) = d(\mathrm{H_{12}-H_{13}}) = d(\mathrm{H_{11}-H_{13}}) = 1.772$ Å (TMAO/NMMO).

TABLE 5: Rigid Substructure Coordinates for the Partly Rigid TMAO Model

atom	*x*/Å	*y*/Å	*z*/Å
O_1	0.000	0.000	0.000
N	0.000	0.000	1.370
C_{1a}	1.396	0.000	1.842
C_{1b}	−0.698	1.209	1.842
C_{1c}	−0.698	−1.209	1.842

TABLE 6: Rigid Substructure Coordinates for the Partly Rigid NMMO Model

atom	*x*/Å	*y*/Å	*z*/Å
O_1	0.000	0.000	0.000
N	0.000	0.000	1.366
C_1	1.394	0.000	1.838
C_{2a}	−0.710	1.213	1.851
C_{2b}	−0.710	−1.213	1.851
C_{3a}	−2.160	1.162	1.407
C_{3b}	−2.160	−1.162	1.407
O_2	−2.778	0.000	1.889
H_{21a}	−0.647	1.257	2.931
H_{21b}	−0.647	−1.257	2.931
H_{22a}	−0.199	2.061	1.413
H_{22b}	−0.199	−2.061	1.413
H_{31a}	−2.206	1.203	0.326
H_{31b}	−2.206	−1.203	0.326
H_{32a}	−2.697	2.005	1.824
H_{32b}	−2.697	−2.005	1.824

(e) Bond and Angle Parameters. Keeping all parameters determined so far fixed, the remaining bond stretching and angle bending terms were adjusted with respect to minimizing the deviations between quantum-chemical and force field *N*-oxide optimal structures and normal vibrations. Using again HF/6-31G** *N*-oxide geometries, the normal frequencies were determined and scaled by the empirical value of 0.893.[53] The force field parameters were optimized again by simulated annealing;[28,39] structural data in the form of atomic distances and vibrational data were weighted equally, and normal modes were assigned by maximizing the overlap between model and reference eigenvectors.

Starting with TMAO, it turned out that the inclusion of Urey−Bradley terms is essential for a reliable representation of structure and normal mode spectrum. With the resulting parameter set given in Tables 7 and 8, the rms deviation between matched force field and ab initio geometry is 0.005 Å, the rms frequency deviation is ca. 50 cm^{-1}. The spectrum is depicted in Figure 3 together with experimental infrared-spectroscopic data by Kuroda and Kimura.[54] More detailed frequency information along with other experimental sources[55,56] is summarized in Table 9, showing excellent agreement. The normal mode quality can be directly attributed to the global optimization technique applied, and any simple local optimization with starting values taken from similar fragments fails.

Keeping parameter transferability to other *N*-oxides in mind, as many TMAO bond and angle terms as possible were used without change for the N−O region in NMMO. Furthermore, the intraring torsional potentials were not modified in anticipation that the spectral adjustment could be accomplished solely

TABLE 7: Harmonic Bond Stretching Parameters: Force Constants k_r^{ab} and Equilibrium Distances r_0^{ab}

type (*a*)	type (*b*)	k_r^{ab}/kcal mol^{-1}Å^{-2}	r_0^{ab}/Å
ON1	NN1	342.58	1.407
ON2	NN2	342.58	1.407
NN1	CT3N1	256.17	1.506
NN2	CT3N2	256.17	1.506
NN2	CT2N	203.57	1.140
CT3N2	CT2N	332.80	1.476
CT3N1	HAN1	590.96	1.082
CT3N2	HAN2	590.96	1.082
CT2N	HAN2	545.45	1.045
CT2NM	ONM	469.03	1.376
CT2NM	HA	499.45	1.060

[a,b] Denote adjacent atoms

by varying the morpholine bend angle potentials. For correctly reproducing the angle between the N−O axis and the ring, it turned out that the O_1-N-C_1 angle parameters had to be released, thereby dropping some transferability of the intramolecular parameters of the N−O region. This is related to the strong electrostatic oxygen−oxygen repulsion that could again in principle be compensated by off-site oxygen charge centers or explicit polarizability. Transferable values were maintained for the parameters of the O_1-N, the $N-C_1$, and the C_1-H_1 bond potentials as well as for the parameters of the $N-C_1-H_1$ angle potential and the corresponding $N-H_1$ Urey−Bradley term. New NMMO parameters had to be derived for the O_1-N-C_1 angle potential and for all bond and angle potentials that imply other morpholine atoms besides nitrogen. Additionally, Urey−Bradley distance potentials for all 1−3 atom pairs except for O_1-C_2 and $N-C_3$ were necessary. With the final parameter set given in Tables 7 and 8, the structural rms deviation between force field and ab initio results is 0.004 Å, and the rms frequency deviation is ca. 48 cm^{-1}. The NMMO spectrum is also depicted in Figure 3, indicating the excellent quality of the intramolecular force field.

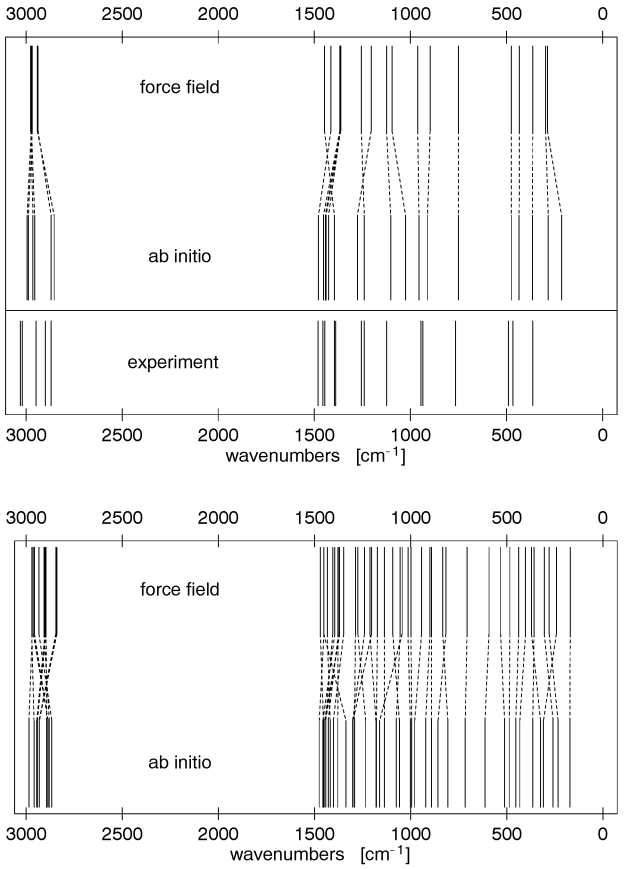

Figure 3. Scaled ab initio and force field normal frequencies of TMAO (top, with experimental IR spectrum[54]) and NMMO (bottom). Dashed lines denote mode assignments.

III. Molecular Dynamics Simulation Results

The complete force field was tested by MD simulations of condensed phases of *N*-oxide/water systems, both crystalline and liquid ones, at various conditions for which experimental data are available. Two model instances were taken into account: The partly rigid model based on the HF/6-31G**-optimized *N*-oxide geometry with local C_3 methyl symmetry, where only the methyl groups are free to rotate under the action of the torsional potential, and the fully flexible model using all parameters described above.

(a) Crystal Structures. Unit cells of NMMO,[52] NMMO monohydrate,[52] di-NMMO-pentahydrate,[57] and TMAO dihydrate[58] were multiplied to yield reasonable simulation boxes (*a*, *b*, *c* multiples were for NMMO: 4 × 5 × 7, NMMO·H_2O: 2 × 6 × 4, 2NMMO·5H_2O: 3 × 6 × 2, TMAO·2H_2O: 4 × 3 ×

TABLE 8: Harmonic Angle Bending and Associated Urey−Bradley 1−3 Stretching Parameters: Force Constants k_α^{abc}/k_r^{ac} and Equilibrium Displacements α_0^{abc}/r_0^{ac} [a]

type (*a*)	type (*b*)	type (*c*)	k_α^{abc}/kcal mol^{-1} rad^{-2}	α_0^{abc}/deg	k_r^{ac}/kcal mol^{-1}Å^{-2}	r_0^{ac}/Å
ON1	NN1	CT3N1	60.94	109.99	72.02	2.330
ON2	NN2	CT3N2	82.46	141.21	72.85	2.034
ON2	NN2	CT2N	44.80	98.31		
NN1	CT3N1	HAN1	49.94	108.07	157.30	2.101
NN2	CT3N2	HAN2	49.94	108.07	157.30	2.101
NN2	CT2N	HAN2	9.09	106.55	184.04	2.158
NN2	CT2N	CT2NM	136.81	97.56		
CT3N1	NN1	CT3N1	137.70	108.16	97.03	2.414
CT3N2	NN2	CT2N	62.06	120.18	151.33	2.565
CT2N	NN2	CT2N	28.83	97.92	44.92	2.103
CT2N	CT2NM	ONM	63.84	112.18	26.00	2.402
CT2NM	ONM	CT2NM	27.10	99.71	4.15	2.026
CT2N	CT2NM	HA	61.21	109.45	69.51	2.171
CT2NM	CT2N	HAN2	76.36	120.32	21.44	1.841
ONM	CT2NM	HA	21.18	109.80	169.20	2.053
HAN1	CT3N1	HAN1	54.87	108.25	13.13	1.768
HAN2	CT3N2	HAN2	54.87	108.25	13.13	1.768
HAN2	CT2N	HAN2	50.03	115.89	14.03	2.026
HA	CT2NM	HA	37.80	117.17	63.81	1.837

[a] *a*−*c* denote adjacent atoms constituting a bend angle.

TABLE 9: Vibrational Frequencies of TMAO: Computed (HF/6-31G, FF: Force Field) and Experimental: (a) Giguère and Chin,[55] (b) Kuroda and Kimura,[54] and (c) Choplin and Kaufmann[56]**

Nr.	type	HF scaled (orig.)	FF	exp.[a]	exp.[b]	exp.[c]
1	A2	213.4 (239.0)	287.0			
2−3	E	282.7 (316.6)	296.7		233	
4−5	E	364.5 (408.1)	364.0	378	380	364
6	A1	434.3 (486.4)	432.7	472	469	466
7−8	E	474.2 (531.1)	475.7	490	497	490
9	A1	749.5 (839.3)	750.8	757−765	756−767	725−759
10	A1	911.1 (1020.2)	897.6	937	936	935
11−12	E	955.5 (1070.0)	962.0	945	946	945
13	A2	1025.3 (1148.1)	1096.1			
14−15	E	1102.5 (1234.6)	1124.4	1135	1124	1124
16	A1	1240.3 (1389.0)	1255.4	1256	1240	1132
17−18	E	1275.8 (1428.7)	1204.0			1241
19−20	E	1395.5 (1562.7)	1447.3	1390	1398	1389
21	A2	1426.0 (1596.9)	1364.5			
22	A1	1438.7 (1611.1)	1362.8	1405	1432	1395
23−24	E	1442.4 (1615.2)	1364.6		1442	1434
25−26	E	1452.3 (1626.3)	1367.0	1458	1457	1473
27	A1	1478.5 (1655.6)	1413.9	1488	1472	1484
28−29	E	2853.8 (3195.7)	2941.5	1668−2285		2870
30	A1	2869.8 (3213.7)	2937.7		2970	
31−32	E	2955.2 (3309.3)	2971.4			2900
33	A1	2964.0 (3319.2)	2975.7	2940	3038	2940
34	A2	2987.9 (3345.9)	2967.5			
35−36	E	2994.4 (3353.2)	2972.7	3012		3020−3030

TABLE 10: Results of *NpT* Simulations and Experimental Crystal Data of NMMO and NMMO Monohydrate (exp., ref 52), Di-NMMO Pentahydrate (exp., ref 57), and TMAO Dihydrate (exp., ref 58) at 293.15K and 1 Bar[a]

	NMMO	NMMO·H_2O	2NMMO·$5H_2O$	TMAO·$2H_2O$
space group	$P2_1/m$	$P2_1/c$	$P2_1/c$	$Pbca$
a(exp.)/Å	9.886	25.481	12.803	9.087
a(partly rigid)/Å	10.213	25.630	12.823	9.182
a(flexible)/Å	10.107	25.751	12.834	9.198
b(exp.)/Å	6.621	6.040	6.500	10.990
b(partly rigid)/Å	6.710	6.220	7.001	10.694
b(flexible)/Å	6.912	6.238	7.032	10.684
c(exp.)/Å	5.112	9.186	21.913	12.778
c(partly rigid)/Å	4.889	8.745	21.129	12.775
c(flexible)/Å	4.913	8.734	21.192	12.796
β(exp.)/deg	111.540	99.880	109.990	90.000
β(partly rigid)/deg	113.812	99.003	114.747	90.005
β(flexible)/deg	114.869	98.915	115.220	90.000
ρ(exp.)/g cm^{-3}	1.250	1.289	1.257	1.157
ρ(partly rigid)/g cm^{-3}	1.269	1.304	1.251	1.177
ρ(flexible)/g cm^{-3}	1.250	1.296	1.245	1.174

[a] Cell parameters $a-c$, monoclinic angle β, average density ρ.

3). The systems were simulated at the experimental conditions of 293.15 K and 1 bar for 100 ps after 150 ps of equilibration. Table 10 shows the simulations results for cell parameters and density along with the experimental values.

The agreement is good, and the differences between partly rigid and fully flexible models are marginal. The densities are on average improved upon using the fully flexible systems and deviate on average by around 1% from the experimental values. The largest discrepancies are observed for the monoclinic angle in the NMMO cases. One can again expect that the single localized point charge on the *N*-oxide oxygen is responsible for this effect: The true charge distribution is slightly shifted off the morpholine ring, accounting for which would induce a change in the relative NMMO orientations. Simulation details of pure TMAO are not given here. All cell parameters agree quite well with the experimental results[44] except for the *a* axis, yielding a density deviation of more than 20%. Given the quality of agreement for all other phases studied, one might speculate that the experimental crystal structure is flawed: The experimental structure consists of antiparallel TMAO layers perpendicular to the *a* axis; the smallest site−site distance observed between the layers is 2.951 Å (hydrogen−hydrogen) while within the layers the shortest distance is 1.615 Å (also hydrogen−hydrogen). Such an anomalously large gap does not exist in the other densely packed *N*-oxide and *N*-oxide hydrate structures.

(b) Density of Liquid Mixtures. A number of simulation for various molar ratios of *N*-oxide/water and two different temperatures have been carried out from which the average densities were obtained. These could be compared with experimental values.[7] For the 1:5 *N*-oxide/water ratio, a total of 840 molecules were used, 1034 for the 1:10 mixture, and 1120 for 1:15. The TMAO 1:10 system corresponds roughly to a 4 M, and the TMAO 1:15 system corresponds to a 3 M solution.[19] Starting with randomly placed molecules, the systems were equilibrated for 400 ps at 1000 K and constant volume at the expected density, and for another 40 ps at the specified temperature and 1 bar followed by 100 ps *NpT* sampling runs. The results are summarized in Table 11.

The agreement between experimental and computational results is generally good, and even better so for NMMO. TMAO solutions tend to be systematically denser than obtained experimentally, whereas NMMO solutions are less dense, although to a lesser percentage. Accounting for full flexibility shows an albeit small yet notably systematic effect for the solutions: The densities in general slightly increase. The smaller the *N*-oxide concentration, the smaller the density deviations as expected, because for small molarity the properties of the water model dominate that is optimized for bulk properties. Further optimization of the *N*-oxide models should focus on the N−O oxygen polarization: As we have seen during the parametrization, with the present point charge model, water molecules do not keep the correct orientation relative to the N−O group. This feature is most likely responsible for the slight increase of the TMAO density.

(c) Liquid Structure of Equimolar Mixtures. We finally turned to conditions for which no experimental information is available but that are most important for the problem of cellulose solubility: Equimolar mixtures of NMMO and water do dissolve cellulose, whereas analogous TMAO solutions do not.[7] We cannot expect to explain these phenomena from structural properties of the solvent alone, but the results will serve as a reference for characterizing the influence of a solute to be studied in the future. Simulation systems were prepared analogously to the dilute solutions: For TMAO/water, 600 molecules were used at 1 bar and a temperature of 533.15 K, above the melting point of the amorphous monohydrate of 474.15 K as reported by Hattori.[59] For the NMMO/water mixtures, 440 molecules were simulated at 1 bar and 373.15 K, the temperature used in industrial cellulose processing, also above the experimental melting point of 345.15 K.[2] The sampling time was 300 ps for each system.

In contrast to the dilute solutions, we observe in the equimolar case a rather strong dependence on the chosen model, more visible for TMAO: The average density from the partly rigid model is 0.672 g cm^{-3}, and for the fully flexible one, it is 0.764 g cm^{-3}. For NMMO, we have 1.065 (partly rigid) and 1.093 g cm^{-3} (fully flexible). Accounting for full flexibility obviously increases the density (by 12% for TMAO and 2.5% for NMMO), as seen before for the dilute systems to a lesser extent. Inter- and intramolecular degrees of freedom strongly couple under these conditions, unexpectedly larger so for TMAO.

TABLE 11: Average Densities ρ from *NpT* Simulations and Experimental Data[7] of Liquid Mixtures of TMAO or NMMO and Water at Various Temperatures *T* and Molar Ratios *N*-Oxide/Water

		molar ratio 1:5		molar ratio 1:10		molar ratio 1:15	
	T/K	298.15	323.15	298.15	323.15	298.15	323.15
TMAO	ρ(exp.)/g cm^{-3}	1.031	1.021	1.014	1.007	1.008	1.001
	ρ(partly rigid)/g cm^{-3}	1.072	1.050	1.046	1.023	1.035	1.013
	ρ(flexible)/g cm^{-3}	1.076	1.054	1.049	1.025	1.037	1.014
NMMO	ρ(exp.)/g cm^{-3}	1.126	1.123	1.084	1.083	1.062	1.063
	ρ(partly rigid)/g cm^{-3}	1.109	1.083	1.078	1.054	1.059	1.034
	ρ(flexible)/g cm^{-3}	1.117	1.090	1.077	1.053	1.063	1.037

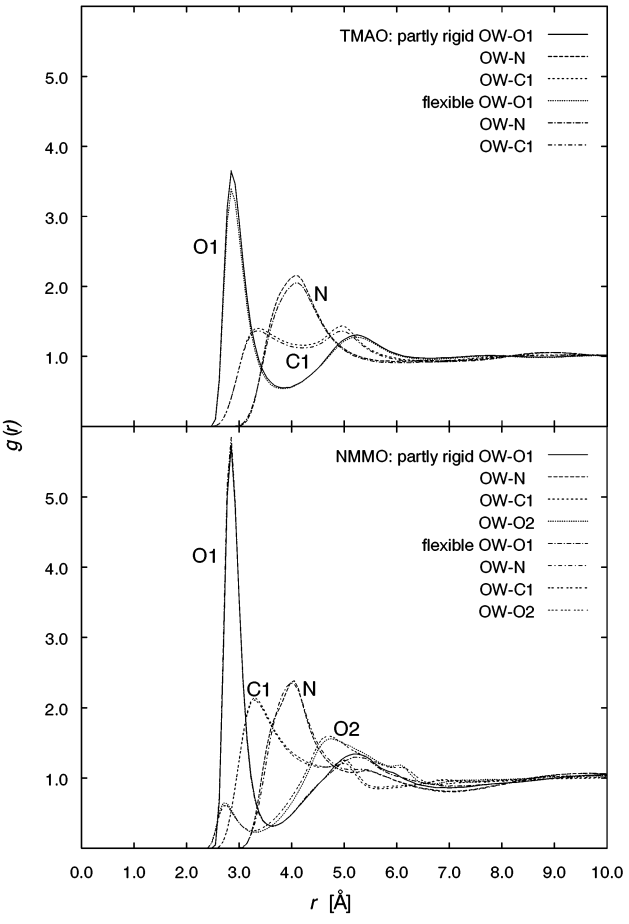

Figure 4. Radial distribution functions of the water oxygen O_W around the *N*-oxide atoms O_1, N, C_1, and O_2 (only for NMMO), for TMAO/water (top) and NMMO/water (bottom).

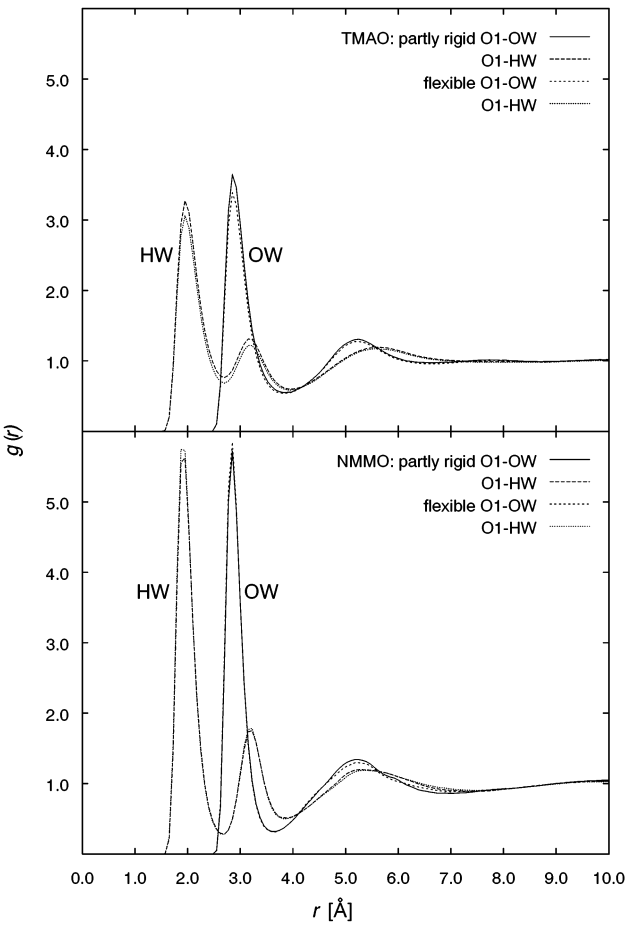

Figure 5. Radial distribution functions of the water oxygen O_W and hydrogen H_W around the *N*-oxide oxygen O_1, for TMAO/water (top) and NMMO/water (bottom).

This phenomenon should also be reflected by the liquid structure that is analyzed here in terms of radial distribution functions, $g(r)$, for various site pairs. In the case of *N*-oxide/water mixtures, the formation of solvent shells of water around the polar N−O bond as well as the positions of *N*-oxides around each other are of great importance. The water oxygen O_W distribution around the atoms of the functional *N*-oxide group O_1, N, C_1 (and for NMMO also O_2 in the morpholine ring) is shown in Figure 4. Concerning the N−O oxygen, two solvent shells at around 2.8 and 5.2 Å can be found which appear to be more pronounced in the NMMO case because of the lower temperature. The distribution around the carbon atom C_1 of the rotatable methyl groups shows for TMAO two weak maxima at around 3.2 and 5.0 Å. For NMMO, the solvation shell is characterized by a single predominant peak. The distribution around the nitrogen atom appears for both systems as a broader maximum at around 4.0 Å. For the ring oxygen O_2 of NMMO also two solvent shells can be identified with the second peak at ca. 4.8 Å as the more pronounced one. This value resembles the O_W−O_2 distance of 4.27 Å found for one of the NMMO monohydrate structures obtained from earlier ab initio calculations[27] where the water molecule is positioned above the morpholine ring bridging both NMMO oxygens. A slight influence of flexibility can be observed in these g functions.

In Figures 5 and 6 (top), the distribution of water sites around the oxygen atoms in TMAO and NMMO is shown. For the oxygen atoms O1 of the N−O group (Figure 5), in both systems, two solvent shells of the water oxygen O_W and three peaks for the corresponding hydrogen atoms H_W can be observed, again more pronounced for NMMO. The corresponding H-bond distances for H_W−O_1 of about 1.9 Å are in good agreement with the results of ab initio calculations of *N*-oxide monohydrates.[27] In Figure 5, the first two peaks for H_W and the first O_W peak can be assigned to the same water molecule. As the first H_W peak is much larger than the second one, an H-bond with a more mobile water molecule can be assumed. The position of this water molecule corresponds to the optimized structure of the monohydrates for TMAO and NMMO.[27]

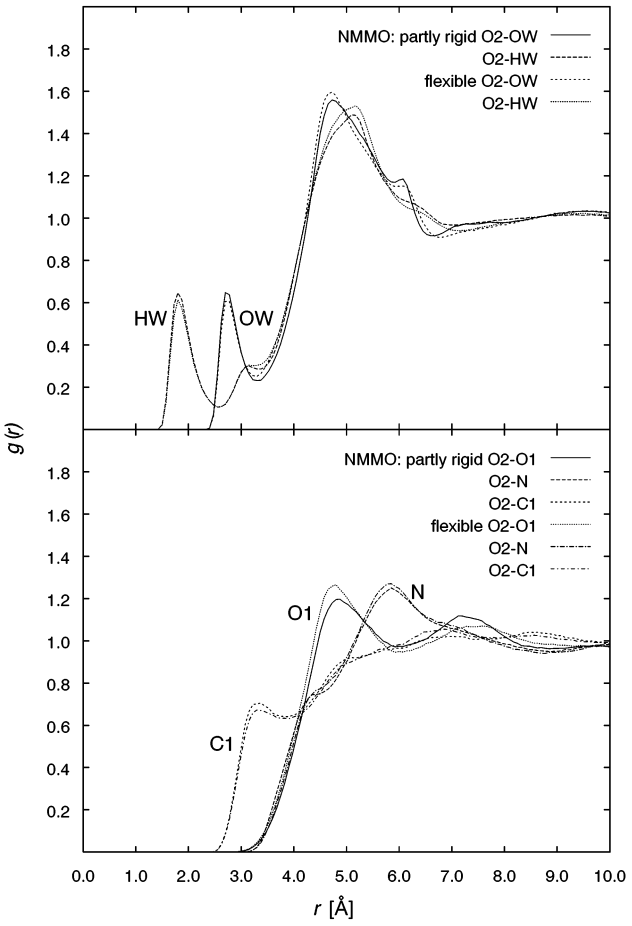

Figure 6. Radial distribution functions of the water oxygen O_W and hydrogen H_W around the NMMO ring oxygen O_2 (top) and of the NMMO atoms O_1, N, and C_1 around the NMMO atom O_2 (bottom).

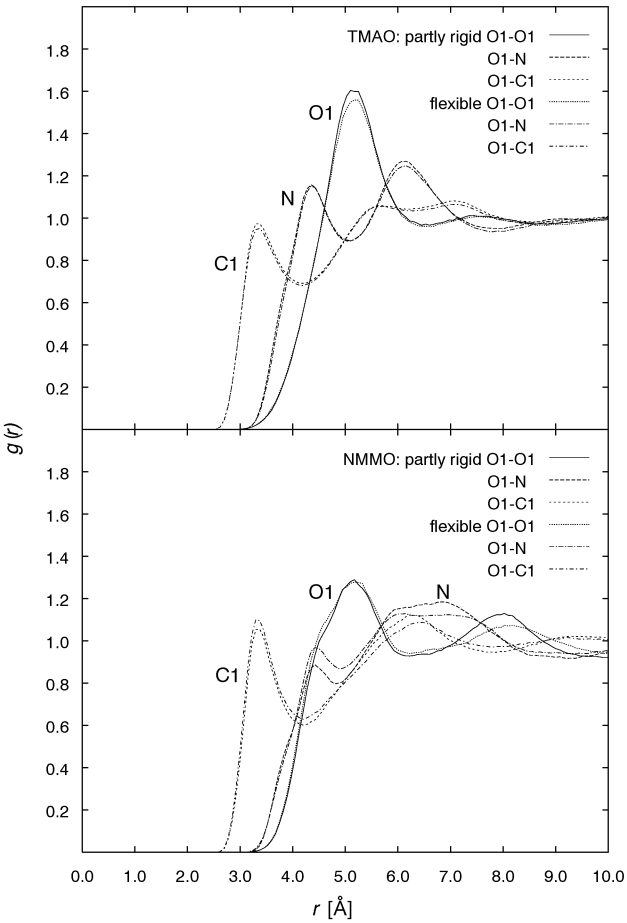

Figure 7. Radial distribution functions of the *N*-oxide atoms O_1, N, and C_1 around the *N*-oxide oxygen O_1, for TMAO/water (top) and NMMO/water (bottom).

By calculating the average amount of O_W atoms in a region of 0−4 Å around O_1, for each of the *N*-oxides, more than one water molecule in the direct neighborhood of the N−O group can be found. For the partly rigid TMAO, we have 1.12 water molecules, whereas the flexible model yields 1.20. For NMMO, the average number of surrounding water molecules increases from 1.28 to 1.32 upon switching to full flexibility. Water is apparently more tightly bound to the N−O group if flexible molecules are present, more so for TMAO than for NMMO. To clarify the physical nature of this effect, we will have to look at intra-/intermolecular cross correlation functions and vibrational/librational mode coupling, for which much larger simulation times will be necessary.

In the case of the morpholine ring oxygen atom O_2 (Figure 6, top), more water molecules can be found in the second solvent shell than in the first one, and it is also spread more broadly. This is a hint for a water position directly above the morpholine ring. Compared to the N−O oxygen O_1, a much smaller number of water molecules can be found in the O_2 region, and the peaks for the partly rigid and the flexible model show slight differences. This effect is even more obvious in the distribution of atoms of the N−O group (O_1, N, and C_1) around the ring oxygen O_2 (Figure 6, bottom). For the carbon C_1 of the rotating methyl group, only a weak solvent shell can be observed around O_2. The peaks for O_1 and N are similarly high and broad. For O_1 on the other hand, there exists another solvent shell that is lower than the first one in the flexible model. The similar height of the main peaks for O_1 and N and the distance between those peaks corresponding to the length of the N−O bond hint at an aligned $O_2\cdots O_1-N$ orientation mediated by water molecules.

Finally, in analogy to the distribution of O_W (Figure 4), the distribution of the methyl group's atoms O_1, N, and C_1 around O_1 is shown in Figure 7. Comparing the results for TMAO and NMMO, both show more than one *N*-oxide coordinated with the O_1 atom. The distribution of the NMMO molecules shows markedly more pronounced differences between the partly rigid and the flexible model than the TMAO distribution due to the flexible ring system. The onset of the peaks at ca. 3 Å point to the existence of bridging water molecules between the *N*-oxides.

IV. Concluding Remarks

The present paper aimed at the development and assessment of an empirical force field for aliphatic *N*-oxides as important cosolvents for water with interesting and still unexplained properties with respect to the stabilization of biomolecules in solution. We have focused on the following key issues: (i) The thorough derivation of potential parameters from a variety of sources by advanced parametrization techniques, (ii) the identification of basic building blocks guiding future parametrization of related species, (iii) providing simulation results as reference material for studies of solvated molecules, and (iv) an assessment of the influence of molecular flexibility as a likely source of genuine *N*-oxide/water mixture properties.

The potential function derived for the two prototypical *N*-oxide species TMAO and NMMO yields single molecule and condensed phase properties in good agreement with available experimental data, given the requirements of simplicity and transferability outlined in the Introduction. Because of the simple functional form chosen, standard parameter combination rules

apply for modeling ternary phases composed of biopolymer species and an *N*-oxide/water solution, allowing for detailed microscopic investigations. With the present force field, first simulations of an oligosaccharide acting as a cellulose model in solvent mixtures of TMAO or NMMO and water have already been conducted,[60] revealing certain H-bond patterns between the carbohydrate and NMMO that could explain the solubility of cellulose in NMMO/water mixtures. Interestingly though, the stabilization of proteins by diluted TMAO appears to be related indirectly to a change of the water structure.[19] The distribution functions for binary mixtures described in this work define a reference based on which the perturbing influence of a polymeric solute can be studied in the future. The remarkable effect of intramolecular *N*-oxide flexibility beyond methyl group rotations that has been observed for binary mixtures appears also to play a role for the solvation process, although no quantitative assessment based for instance on free energy computations has been attempted yet. Detailed discussions of the flexibility problem will require much more expensive simulations than were performed in the present work.

The final parameter set serves as good starting point for the parametrization of other *N*-oxides: Keeping various terms unchanged that have been identified as being transferable, future force field development can focus solely on unknown parts of the compounds under consideration. The available evidence gathered throughout the parametrization and validation process points to a key limitation of the present force field that needs to be addressed in future work: The simple point charge model of the *N*-oxide oxygen appears not to be capable of describing the physical situation satisfactorily; adding a polarization term will be necessary to account for certain structural features of pure and hydrated *N*-oxides. Another issue to consider is the water model that has been restricted in this work to the rigid TIP3P form optimized for the neat liquid: One not only needs to address the problem of parameter validity at high cosolvent concentration but also the intramolecular water dynamics that appears to be modulated in the presence of TMAO, as indicated by a recent infrared-spectroscopic study.[18] It will be interesting to see what level of physical detail is necessary to explain the genuine *N*-oxide effects on biopolymer stability.

A number of open questions can only be answered by appropriate experiments performed on *N*-oxide/water mixtures. For instance, frequencies and amplitudes of isotopically substituted species should give rise to different structures and thermodynamics. Equally important would be information about the dielectric constants for various mixtures as well as studies with respect to a separation of intramolecular and intermolecular correlation functions that could be directly compared with simulation data. Perhaps this work can inspire some experimental effort.

Acknowledgment. This work was supported by the *Deutsche Forschungsgemeinschaft* within the Schwerpunktprogramm "Cellulose und Cellulosederivate - molekulares und supramolekulares Strukturdesign". S.M.K. thanks the Alexander von Humboldt-Stiftung for financial support. Bernd Schilling provided the programs for computing the radial distribution functions.

References and Notes

(1) Chanzy, H.; Dubé, M.; Marchessault, R. H. *J. Polym. Sci.: Polym. Lett. Ed.* **1979**, *17*, 219.

(2) Chanzy, H.; Nawrot, S.; Péguy, A.; Smith, P. *J. Polym. Sci.: Polym. Phys. Ed.* **1982**, *20*, 1909.

(3) Chanzy, H.; Noe, P.; Paillet, M.; Smith, P. *J. Appl. Polym. Sci.: Appl. Polym. Symp.* **1983**, *37*, 239.

(4) Taeger, E.; Michels, C.; Nechwatal, A. *Das Papier* **1991**, *12*, 784.

(5) Creely, J. J.; Wade, R. H.; French, A. D. *Text. Res. J.* **1978**, *48*, 37.

(6) Philipp, B.; Schleicher, H.; Wagenknecht, W. *Chem. Technol.* **1977**, *11*, 702.

(7) Akzo Nobel, Obernburg, private communication.

(8) Yancey, P. H.; Somero, G. N. *J. Exp. Zool.* **1980**, *212*, 205.

(9) Yancey, P. H.; Clark, M. E.; Hand, S. C.; Bowlus, R. D.; Somero, G. N. *Science* **1982**, *217*, 1214.

(10) Yancey, P. H.; Siebenaller, J. F. *J. Exp. Biol.* **1999**, *202*, 3597.

(11) Eidenmüller, K.; Fath, T.; Hellwig, A.; Reed, J.; Sontag, E.; Brandt, R. *Biochemistry* **2000**, *39*, 13166.

(12) Anthoni, U.; Christophersen, C.; Gajhede, M.; Nielsen, P. H. *Struct. Chem.* **1992**, *3*, 121.

(13) Lin, T. Y.; Timasheff, S. N. *Biochemistry* **1994**, *33*, 12695.

(14) Wang, A.; Bolen, D. W. *Biochemistry* **1997**, *36*, 9101.

(15) Baskakov, I. V.; Bolen, D. W. *J. Biol. Chem.* **1998**, *273*, 4831.

(16) Baskakov, I. V.; Kumar, R.; Srinivasan, G.; Ji, Y.; Bolen, D. W.; Thompson, E. B. *J. Biol. Chem.* **1999**, *274*, 10693.

(17) Palmer, H. R.; Bedford, J. J.; Leader, J. P.; Smith, R. A. J. *J. Biol. Chem.* **2000**, *275*, 27708.

(18) Sharp, K. A.; Madan, B.; Manas, E.; Vanderkooi, J. M. *J. Chem. Phys.* **2001**, *114*, 1791.

(19) Zou, Q.; Bennion, B. J.; Daggett, V.; Murphy, K. P. *J. Am. Chem. Soc.* **2002**, *124*, 1192.

(20) Noto, R.; Martorana, V.; Emanuele, A.; Fornili, S. L. *J. Chem. Soc., Faraday Trans.* **1995**, *91* 3803.

(21) Stare, J.; Mavri, J.; Ambrožič, G.; Hadži, D. *J. Mol. Struct. (THEOCHEM)* **2000**, *500*, 429.

(22) Došlić, N.; Stare, J.; Mavri, J. *Chem. Phys.* **2001**, *269*, 59.

(23) Brooks, B. R.; Bruccoleri, R. E.; Olafsen, B. D.; States, D. J.; Swaminathan, S.; Karplus, M. *J. Comput. Chem.* **1983**, *4*, 187.

(24) Nilsson, L.; Karplus, M. *J. Comput. Chem.* **1986**, *7*, 591.

(25) MacKerell, A. D., Jr.; Bashford, D.; Bellott, R. L.; Dunbrack, R. L., Jr.; Evanseck, J. D.; Field, M. J.; Fischer, S.; Gao, J.; Guo, H.; Ha, S.; Joseph-McCarthy, D.; Kuchnir, L.; Kuczera, K.; Lau, F. T. K.; Mattos, C.; Michnick, S.; Ngo, T.; Nguyen, D. T.; Prodhom, B.; Reiher, W. E., III.; Roux, B.; Schlenkrich, M.; Smith, J. C.; Stote, R.; Straub, J.; Watanabe, M.; Wiorkiewicz-Kuczera, J.; Yin, D.; Karplus, M. *J. Phys. Chem. B* **1998**, *102*, 3586.

(26) Reiling, S.; Schlenkrich, M.; Brickmann, J. *J. Comput. Chem.* **1996**, *4*, 450.

(27) Kast, K. M.; Reiling, S.; Brickmann, J. *J. Mol. Struct. (THEOCHEM)* **1998**, *453*, 169.

(28) Kast, S. M.; Brickmann, J.; Berry, R. S. In *Conceptual Perspectives in Quantum Chemistry*; Calais, J. L., Kryachko, E., Eds.; Kluwer: Dordrecht, The Netherlands, 1997; p 195.

(29) Norrby, P.-O.; Liljefors, T. *J. Comput. Chem.* **1998**, *19*, 1146.

(30) Wang, J.; Kollman, P. A. *J. Comput. Chem.* **2001**, *22*, 1219.

(31) Henderson, D. *Annu. Rev. Phys. Chem.* **1974**, *25*, 461.

(32) Steinbach, P. J.; Brooks, B. R. *J. Comput. Chem.* **1994**, *15*, 667.

(33) Frisch, M. J.; Trucks, G. W.; Schlegel, H. B.; Gill, P. M. W.; Johnson, B. G.; Robb, M. A.; Cheeseman, J. R.; Keith, T.; Petersson, G. A.; Montgomery, J. A.; Raghavachari, K.; Al-Laham, M. A.; Zakrzewski, V. G.; Ortiz, J. V.; Foresman, J. B.; Cioslowski, J.; Stefanov, B. B.; Nanayakkara, A.; Challacombe, M.; Peng, C. Y.; Ayala, P. Y.; Chen, W.; Wong, M. W.; Andres, J. L.; Replogle, E. S.; Gomperts, R.; Martin, R. L.; Fox, D. J.; Binkley, J. S.; Defrees, D. J.; Baker, J.; Stewart, J. P.; Head-Gordon, M.; Gonzalez, C.; Pople, J. A. *Gaussian 94*; Gaussian, Inc.: Pittsburgh, PA, 1995.

(34) Boys, S. F.; Bernadi, F. *Mol. Phys.* **1970**, *19*, 553.

(35) Kast, S. M.; Brickmann, J. *J. Chem. Phys.* **1996**, *104*, 3732.

(36) Berendsen, H. J. C.; Postma, J. P. M.; van Gunsteren, W. F.; DiNola, A.; Haak, J. R. *J. Chem. Phys.* **1984**, *81*, 3684.

(37) Ryckaert, J.-P.; Ciccotti, G.; Berendsen, H. J. C. *J. Comput. Phys.* **1977**, *23*, 327.

(38) Ciccotti, G.; Ferrario, M.; Rykaert, J.-P. *Mol. Phys.* **1982**, *55*, 549.

(39) Hauptmann, S.; Dufner, H.; Brickmann, J.; Kast, S. M.; Berry, R. S. *Phys. Chem. Chem. Phys.* **2003**, *5*, 635.

(40) Linton, E. P. *J. Am. Chem. Soc.* **1940**, *62*, 1945.

(41) Phillips, G. M.; Hunter, J. S.; Sutton, L. E. *J. Chem. Soc.* **1945**, 146.

(42) Dufner, H.; Kast, S. M.; Brickmann, J.; Schlenkrich, M. *J. Comput. Chem.* **1997**, *18*, 660.

(43) Ewald, P. P. *Ann. Phys.* **1921**, *64*, 253.

(44) Caron, A.; Palenik, G. J.; Goldish, E.; Donohue, J. *Acta Crystallogr.* **1964**, *17*, 102.

(45) Jorgensen, W. L. *J. Am. Chem. Soc.* **1981**, *103*, 335.

(46) Jorgensen, W. L.; Chandrasekhar, J.; Madura, J. D.; Impey, R. W.; Klein, M. L. *J. Chem. Phys.* **1983**, *79*, 926.

(47) Reiher, W. E., III. Ph.D. Thesis, Harvard University, Cambridge, MA, 1985.
(48) Ferro, D. R.; Hermans, J. *Acta Crystallogr*. **1977**, A *33*, 345.
(49) Jordan, P. C.; van Maaren, P. J.; Mavri, J.; van der Spoel, D.; Berendsen, H. J. C. *J. Chem. Phys.* **1995**, *103*, 2272.
(50) Kaminski, G. A.; Stern, H. A.; Berne, B. J.; Friesner, R. A.; Cao, Y. X.; Murphy, R. B.; Zhou, R.; Halgren, T. A. *J. Comput. Chem.* **2002**, *23*, 1515.
(51) Press, W. H.; Teukolsky, S. A.; Vetterling, W. T.; Flannery, B. P. *Numerical Recipes in Fortran*, 2nd ed.; Cambridge University Press: Cambridge, 1992.
(52) Maya, E.; Peguy, A.; Pérez, S. *Acta Crystallogr*. **1981**, B *37*, 1858.
(53) Pople, J. A.; Krishnan, R.; Schlegel, H. B.; DeFrees, D.; Binkley, J. S.; Frisch, M. J.; Whiteside, R. F.; Hout, R. F.; Hehre, W. J. *Int. J. Quantum Chem., Quantum Chem. Symp.* **1981**, *15*, 269.
(54) Kurodo, Y.; Kimura, M. *Spectrochim. Acta* **1966**, *22*, 47.
(55) Giguère, P. A.; Chin, D. *Can. J. Chem.* **1961**, *39*, 1214.
(56) Choplin, F.; Kaufmann, G. *Spectrochim. Acta* **1970**, *26A*, 2113.
(57) Maya, E.; Pérez, S. *Acta Crystallogr*. **1982**, *B 38*, 848.
(58) Mak, T. C. W. *J. Mol. Struct.* **1988**, *178*, 169.
(59) Hattori, Y. *J. Pharm. Soc. Jpn.* **1940**, *60*, 24.
(60) Marhöfer, R. J.; Kast, K. M.; Schilling, B.; Bär, H.-J.; Kast, S. M.; Brickmann, J. *Macromol. Chem. Phys.* **2000**, *201*, 2003.